JMEPEG (2024) 33:9850–9860
https://doi.org/10.1007/s11665-024-09518-z

©The Author(s)
1059-9495/$19.00

ORIGINAL RESEARCH ARTICLE

Synthesis of Medium Entropy Coatings and Study of the Influence of Bias Voltage and Nitrogen Flow on Their Microstructural and Tribological Properties

M. Alejandro Grisales, M. Daniela Chimá, and G. Bejarano Gaitán

Submitted: 20 February 2023 / Revised: 11 December 2023 / Accepted: 21 March 2024 / Published online: 7 June 2024

TiTaZrNb medium entropy coatings and their nitride forms (TiTaZrNb)Nx were synthesized by direct current magnetron sputtering. The study evaluated the bias voltage affects microstructure, chemical and phase composition of the metallic coatings. Also, the effect of nitrogen flow on the microstructural and tribological properties of the corresponding nitrides was studied. A change in the crystalline structure from BCC for TiTaZrNb coatings to FCC for (TiTaZrNb)Nx was observed. It was associated with the incorporation of nitrogen into the matrix and the consequent formation of a solid solution of (TiTaZrNb)Nx. An increase in the hardness and residual stresses of the metallic coating was observed with increasing bias voltage to − 130 V and of the nitride coating with increasing nitrogen flow to 12 sccm, reaching hardness values of 12.8 GPa and 25 GPa, respectively. A slight reduction in the hardness of the deposited nitride coating was observed at the higher nitrogen flow of 15 sccm, probably due to the formation of the TiN and ZrN phases. The higher hardness and lower wear rate of the (TiTaZrNb)Nx nitride coatings compared to the uncoated M2 steel samples demonstrate the protective effect against wear of these coatings.

Keywords coatings, entropy, inorganic, medium, nitride, tribology

1. Introduction

High entropy alloys (HEA) and high entropy alloy coatings (HEAc) are a novel materials made up of five or more elements in quasi-equimolar or equiatomic amounts. They commonly form a solid solution of a single body-centered cubic (BCC) or face-centered (FCC) phase, or a combination of both (Ref 1). Similar alloys with only four elements, called medium entropy alloys (MEAs), have also been developed (Ref 2-4). The high entropy of the alloy results from the sum of the entropies of the individual elements. This leads to exceptionally high physical, chemical and mechanical properties that could not be obtained with conventional materials and alloys (Ref 5).

The properties of HEAs arise from a synergistic combination of physicochemical phenomena known as the "cocktail effect" (Ref 6). This effect is a result of various factors, including the high concentration of vacancies in the solid solution due to the solubility between alloy's constituent elements. Additionally, significant deformation in the crystal lattice, stacking faults, reduced dislocation mean free path and decrease in oxygen diffusion coefficient within the matrix (Ref 7, 8).

The inclusion of atoms with smaller atomic sizes like nitrogen and carbon in the matrix alloy leads to the formation of solid solutions of ceramic character with significant lattice deformation. When the solubility limit of the matrix is surpassed, other nitrides, carbides and carbonitrides could be formed (Ref 9), which further can increase the mechanical and tribological properties, as well as the oxidation resistance of the alloys (Ref 8, 10-12).

One of the commonly employed techniques for fabricating HEAs and MEAs coatings is magnetron sputtering. It is preferred due to its favorable attributes, including the ability to produce high-quality films, achieve a desirable deposition rate, ensure good adhesion, and enable control over coating properties through process parameters (Ref 13). Specifically, the application of a bias voltage can significantly impact properties such as composition, hardness and density. This is primarily due to the increased energy of ions bombarding the surface, which enhances the substrate ability to engage in chemical reaction on its surface. In their study, Cemin et al (Ref 14) investigated the impact of substrate bias on the mechanical and microstructural properties of magnetron sputtered NbTaTiVZr coatings. The results revealed that an increase in bias voltage led to an enhancement in hardness. Furthermore, the surfaces exhibited higher roughness and a shift in the crystal orientation was observed from body-centered cubic (BCC) 110-200. Similarly, Xu et al (Ref 15) conducted a study investigating the effect of increasing bias voltage on the hardness of (AlCrTiVZr)N films. They attributed the hardness improvement to the grain refinement strengthening mechanism that occurs at higher bias values. Additionally, the densification process reduced the presence of voids between columns and grains. The

M. Alejandro Grisales, M. Daniela Chimá, and **G. Bejarano Gaitán**, Centro de Investigación, Innovación y Desarrollo Tecnológico CIDEMAT, Facultad de Ingeniería, Universidad de Antioquia, Medellín, Colombia. Contact e-mail: malejandro.grisales@udea.edu.co.

crystal orientation of the films shifted from 200 at lower bias values to 111 at higher bias values.

Another crucial process parameter to consider in relation to nitride coatings is N_2 flow. El Garah et al (Ref 16) explored the correlation between the microstructure and composition of AlTiTaZr(-N) magnetron sputtered films. Their study revealed that films produced at lower nitrogen flow rated exhibited amorphous structures. In contrast, as the nitrogen flow increased, the microstructure transformed into a face-centered cubic (FCC) solid solution with a remarkable hardness of up to 24.6 GPa. Bachani et al (Ref 17) examined the effects of varying nitrogen flow on the microstructure, hardness and tribological properties of (TiZrNbTaFe)N coatings deposited by high power impulse magnetron sputtering (HiPIMS). The N_2 flow (N_2/(N_2 + Ar)) ratio was varied from 0 to 33.3%. The absence or low nitrogen ratios resulted in the formation of amorphous films, while an increase in nitrogen content led to the development of an FCC solid solution with a nanocrystalline nitride phase. The authors observed that both hardness and friction coefficient exhibited variations in response to N_2 flow. Notably, the authors reported a hardness of 36.2 GPa, accompanied by low wear rates, good adhesion and corrosion resistance when the N_2 flow was set to 3 sccm (10% N_2 ratio).

In their study, Shu et al (Ref 18) presented the synthesis of near-stoichiometric (TiNbZrTa)N_x coatings and investigated the impact of nitrogen content on the microstructure and corrosion resistance. The hardness values reported ranged from 5 to 23 GPa depending on the nitrogen flow rate. Transformation of the microstructure from BCC phase to FCC phase upon transitioning from the metallic to the nitride form. Moreover, the corrosion resistance of the coating was found to be strongly influenced by the nitrogen content. However, as of the authors knowledge, no previous studies have been published on the mechanical and tribological properties of TiTaZrNb and (TiTaZrNb)N coatings, which are potentially suitable for anti-wear applications. Consequently, a knowledge gap exists regarding these coating's characteristics.

Considering the aforementioned knowledge gap, this study aimed to synthesize the MEA coating system TiTaZrNb and its corresponding nitride (TiTaZrNb)N. The investigation focused on evaluating the impact of bias voltage on TiTaZrNb as matrix coating and the effect of nitrogen flow on the microstructural, mechanical and tribological properties of these coatings. By conducting this study, valuable insights can be gained into the properties and potential applications of TiTaZrNb and (TiTaZrNb)N coatings.

2. Experimental Details

2.1 Substrate Preparation

AISI M2 steel substrates commonly utilized in the fabrication of cutting and forming tools with an average hardness of 62 HRC were selected. Additionally, (100) oriented silicon wafers were employed for specific characterization techniques. The steel samples were roughed using sandpaper ranging from 240 to 1500 grit, followed by mirror polished with alumina with particle sizes of 1.0 and 0.05 μm. Subsequently, the samples were subjected to a 30-minute ultrasonic bath in a solution containing ethanol and acetone. Finally, an ionic cleaning of the samples was carried out inside the coating chamber for 45 minutes, supplying a bias voltage of − 650 V, using an argon atmosphere at a pressure of 1.0 Pa and a temperature of 250 °C.

2.2 TiTaZrNb and (TiTaZrNb)N_x Coatings Deposition

MEA metallic coatings were deposited onto the steel substrates using a TiTaZrNb alloy target with 25 at.% of each element with a purity of 99,9% (Manufacturer Able Target Limited). The target dimensions were 500 mm height, 100 mm width and 5 mm thickness. The samples were positioned 90 mm away from the target and rotated at 12 rpm. The process parameters, which are shown in Table 1, included varying the bias voltage while maintaining constant pressure and temperature. Prior to TiTaZrNb deposition, a Ti/TiN bilayer with a thickness of 200 nm was applied to enhance adhesion between the coating and substrate. For the TiN deposition, a nitrogen flow of 9 sccm was introduced.

For the synthesis of MEA nitride coating, the same process parameters were used as for the deposition of the TiTaZrNb matrix, maintaining a constant bias of − 70 V and varying the nitrogen flow to evaluate its influence on the microstructural, mechanical and tribological properties of these coatings. The N_2 flow rates used to synthesize the RN1, RN2 and RN3 coatings were 9, 12 and 15 sccm, respectively, as resumed in Table 1. Bias values greater than − 70 V were discarded, since they generated detachment of the coating.

2.3 Characterization of the Coatings

The surface area and cross section of the deposited coatings were evaluated on a JEOL JSM-6490LV scanning electron microscope (SEM). Elemental composition was determined by energy-dispersive x-ray spectroscopy (EDX), using a microprobe built into the SEM and with help of INCA Energy software.

Roughness of coatings was determined with an MFP-3D Infinity Asylum Research atomic force microscope (AFM) in three different zones with a scan of 5 μm^2. For this purpose, a silicon tip and contact mode were used. The microstructural and phase analysis of the coating was carried out in a Panalytical Empyrean x-ray diffractometer using a Cu Kα source with λ = 1.540598 Å, 45 kV, 40 mA, with an incidence angle of 1° and a step of 0.02° per second. The diffraction patterns were analyzed with the HighScore Plus software. The transmission electron microscopy was carried out with a FEI TECNAI F20 SUPER TWIN TMP microscope with an acceleration voltage of 200 kV. Gatan digital micrograph software was used to measure d-spacing and FFT images.

Rockwell C indentation method was used to qualitatively measure the adherence of coatings. 4 indentations were performed on 2 samples of each coating at a force of 150 kgf with a diamond cone indenter. The microhardness of the coated samples was determined by Vickers method in a Shimadzu hardness tester HMV-G 21 applying a load of 0.294 N (0.030 kgf/mm^2) for 30 seconds.

The residual stresses of the coatings deposited on single-crystalline silicon wafers were determined by measuring the radius of curvature before and after coating deposition using Stoney's Eq 1. (Ref 19). For each coating, 6 measurements were taken in a Bruker brand contact profilometer with a load of 3 mN for 120 seconds and a distance of 2.5 cm.

Table 1 Processing parameters for the TiTaZrNb and (TiTaZrNb)Nx coatings

Sample	TiTaZrNb Power kW	Ar flow sccm	N_2 flow sccm	N_2/Ar Ratio (N_2/Ar + N_2) %	Time min	Temperature °C	Bias V	Pressure Pa
R1	1.7	38	…	…	120	320	− 70	0.2
R2							− 100	
R3							− 130	
R4							− 160	
RN1	1.3	38	9	19	180	320	− 70	0.2
RN2			12	24				
RN3			15	28				

$$\sigma = \frac{E_s.T^2{}_s}{6.T_f}\left(\frac{1}{R_1} - \frac{1}{R_0}\right) \quad \text{(Eq 1)}$$

where E_s (with 180.3 GPa) and T_s are the Young's modulus and the thickness of the silicon wafer, T_f is the thickness of the coating, and R_o and R_1 are the radii of curvature of the silicon wafer before and after the coating.

The tribological behavior of the (TiTaZrNb)Nx coatings was determined under the ASTM G99-17 standard (Ref 20) using a ball-on-disk type tribometer with a 6-mm-diameter alumina ball as a counterbody. The applied load was 3N for 13 minutes for a sliding distance of 5 m. The diameter of the wear mark was 4 mm, and the rotation speed of the substrate was 30 rpm. The wear track profile was determined using a Bruker Dektakxt contact profilometer, and its volume was calculated from equation $V = A * 2\pi * r$. V is the volume in mm^3, A is the cross-sectional area in mm^2, and r is the radius of the wear track in mm. The wear rate was determined using the equation $k = \frac{V}{F.l}$, where k is the wear rate, V is the worn volume in mm^3, F is the load applied in N, and L is the sliding distance in m.

3. Results and Discussion

3.1 TiTaZrNb Coatings

Figure 1 shows cross-sectional images of the TiTaZrNb coatings deposited with different bias voltages. A typical columnar growth structure of coatings synthesized by physical vapor deposition (PVD) techniques is observed. It is also possible to see a slight decrease in the width of the columns and an increase in the density of the coatings associated with the higher bias voltage. This behavior can be attributed to the increased kinetic energy and mobility of ions involved in coating formation. According to the structure zone model (SZM), all the coatings exhibit the characteristic structure of zone T, which is characterized by columns accompanied by smooth surfaces (Ref 21). The higher kinetic energy facilitates greater superficial diffusion, allowing for enhanced adatom movement within the coating. Additionally, the elevated mobility of ions contributes to the generation of a higher density of nucleation sites, which in turn promotes the formation of grains and columns within the coating structure (Ref 22). This phenomenon has been observed in previous works, Wei Dai et al. who deposited TaN by sputtering varying the bias voltage between 0 and − 300 V (Ref 23). Their findings aligned with the present study, demonstrating similar trends in coating characteristics. Furthermore, Jian-Fu Tang and colleagues (Ref 24) deposited CrAlN coatings on M2 high-speed steel substrates using HiPIMS. They observed notable effects of bias voltage on the resulting coatings, including grain refinement, coating densification, increased hardness, and residual stresses.

The elemental composition obtained by EDX is presented in Table 3. The composition of the coatings closely aligns with that of the TiTaZrNb- target (25 at.% of each element). A slight decrease in the percentages of Ti and Zr is seen with increasing bias voltage. This phenomenon can be attributed to a resputtering effect, which occurs due to the lower chemical bond strength of these elements and their lower melting points compared to Nb and Ta. Resputtering, characterized by the preferential removal of lighter elements, has also been observed in previous studies. For example, Lin et al (Ref 12) reported similar findings in the deposition of (CrAlNbSiV)N HEA coating, where variation in bias and nitrogen ratio resulted in an increased composition of heavier elements through the removal of lighters elements. Other researchers have also reported comparable observations in the fabrication of nitride coatings (Ref 23, 24). Oxygen content is seen in all the coatings due to the traces of this element contained in the targets and in the vacuum chamber that cannot be completely evacuated. In addition, nanolayers of oxides form on the surface of the samples during their handling time.

The crystal structure of the TiTaZrNb coatings was examined using x-ray diffraction (XRD). Figure 2 shows the diffraction patterns obtained from coatings deposited at different bias voltages. The XRD analysis revealed that all coatings exhibited a single crystalline BCC phase of TiTaZrNb with preferential growth in the (110) plane. This result is consistent with previous Nb(Ta)TiZr laser clad coatings reported by Guan et al (Ref 25) and magnetron sputtered quaternary TiNbTaZr coating fabricated by S. Achache (Ref 26). These studies demonstrated that TiTaZrNb develop a BCC cubic structure, irrespective of the stoichiometry and process parameters during the fabrication process. Furthermore, a slight shift in the diffraction angle was observed with increasing bias voltage. This behavior can be attributed to the presence of tensile-type residual stresses within the coating. The increase in bias voltage leads to enhanced ion energy and mobility, resulting in denser coating and generating tensile stresses, as shown in Fig. 3.

Figure 3 illustrates the variation of residual stresses and adherence in the TiTaZrNb coatings as a function of bias voltage, as calculated using the Stoney equation and Rockwell C indentation. The results show that the residual stresses increase with increasing bias voltage. Specifically, a tensile-

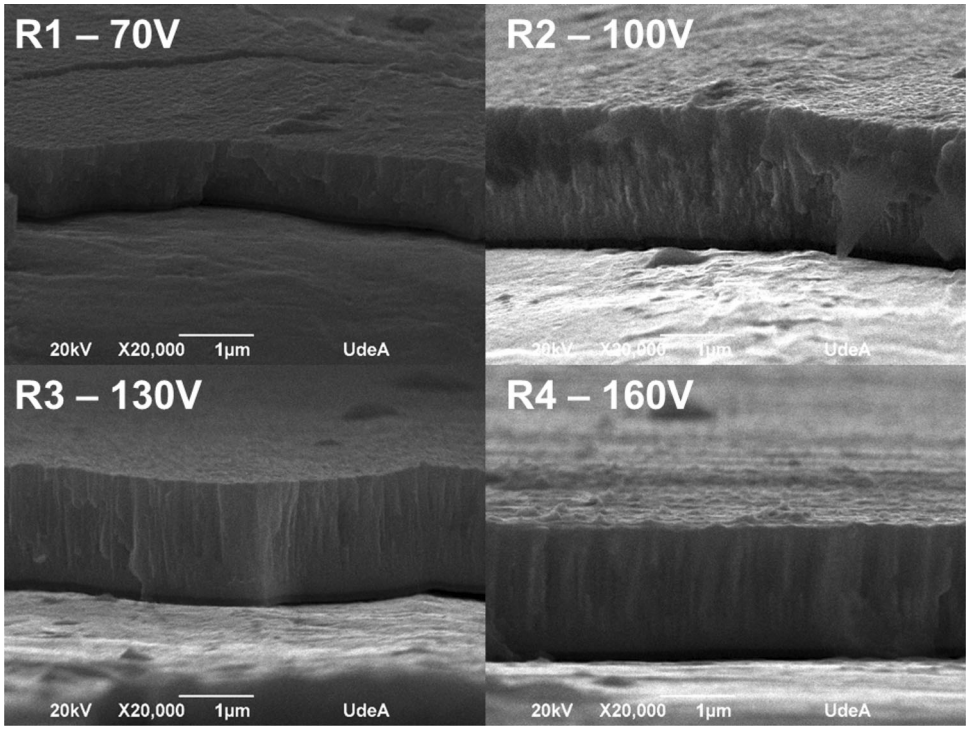


Fig. 1 Cross-sectional SEM images of TiTaZrNb coatings deposited at different bias voltages

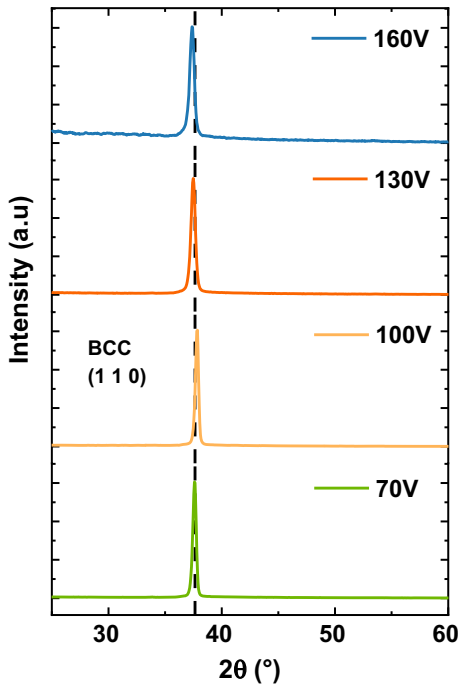


Fig. 2 Diffraction patterns of TiTaZrNb coatings deposited with different bias voltages

type stress is observed, ranging from 2 GPa for films deposited at − 70 V to approximately 8 GPa for films deposited at a bias of − 160 V. Although the quantitative determination of coating-substrate adhesion was not performed in this study, it was observed that the coating deposited at a bias of − 160 V experienced detachment from the substrate shortly after the samples were removed from the vacuum chamber. This observation aligns with previous reports indicating that the adhesion strength of coatings decreases with increasing residual stresses. It is worth nothing that films with residual stresses close to 10 GPa often lead to complete detachment from the substrate (Ref 27).

Figure 4 depicts the relationship between microhardness and bias voltage in the TiTaZrNb coatings. The results show an increasing trend in microhardness with increasing bias voltage up to − 130 V, followed by a slight decrease. The hardness values ranged between 10-14 GPa, which is consistent with similar metallic sputtered HEA films (Ref 14, 26, 28). However, it should be noted that these results may be influenced by the hardness of the substrate, as indicated by the 0.294N load used in the measurements. The observed increase in hardness can be attributed to several factors. Firstly, the high entropy mixture of the alloy, characterized by a single-phase solid solution, contributed to the enhanced hardness. Additionally, the deformation of the crystalline lattice, reflected in the increase in residual stresses, and the possible densification of the coating due to intense ionic bombardment are contributing factors (Ref 23, 24, 29). However, at higher bias voltages (− 160 V), a decrease in mean microhardness is observed. This can be attributed to two main factors. Firstly, the resputtering of Ti and Zr is due to high kinetic energy of ions bombarding the growing coating, as evidenced by the elemental composition in Table 2. Secondly, previous studies have indicated that higher bias voltages lead to an increase in grain size (Ref 29). According to the Hall–Petch equation, an increase in grain size leads to a reduction in hardness (Ref 30). Additionally, the increase in temperature identified at bias conditions can promote the recovery of some defects within the crystalline network, further influencing the reduction in hardness. However, in this case, such a phenomenon is not observed, as the residual stresses continue to increase with applied bias voltage.

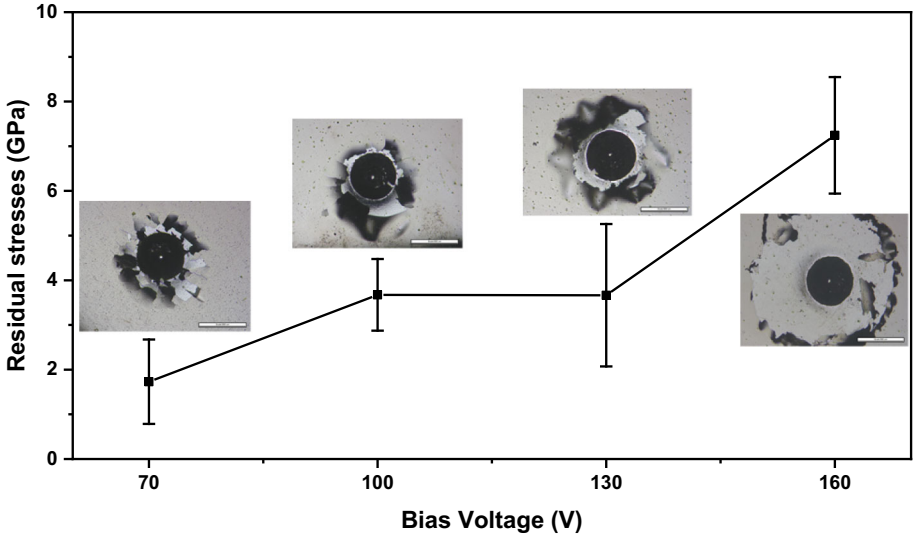


Fig. 3 Tensile-type residual stresses in the TiTaZrNb coating as a function of the bias voltage applied to the substrate

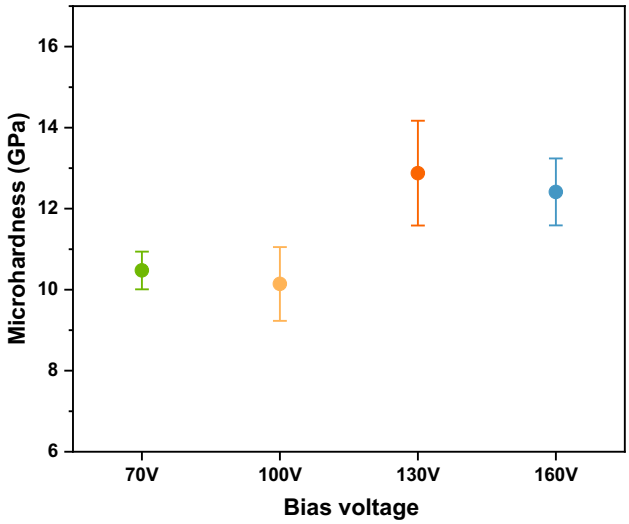


Fig. 4 Microhardness of the synthesized TiTaZrNb coatings

Table 2 Elemental chemical composition (%.at.) of the TiTaZrNb coatings deposited at different bias voltages

	Bias			
Element	**− 70, V**	**− 100, V**	**− 130, V**	**− 160, V**
Ti	24.1 ± 0.1	23.3 ± 0.1	21.9 ± 0.4	22.0 ± 0.4
Zr	19.9 ± 0.3	19.4 ± 0.3	20.5 ± 0.3	19.7 ± 0.1
Nb	23.0 ± 0.1	23.8 ± 0.3	24.0 ± 0.2	25.0 ± 0.4
Ta	24.8 ± 0.2	25.9 ± 0.3	25.7 ± 0.2	26.7 ± 0.4
O	8.2 ± 0.2	7.6 ± 0.1	7.8 ± 0.4	6.6 ± 0.5

3.2 (TiTaZrNb)N_x Coatings

Cross-sectional SEM images of TiTaZrNb nitride coatings are shown in Fig. 5. The coatings exhibit a dense columnar structure with an approximate thickness of 2 microns. Although the exact thickness is not easily discernible from the SEM images due to sample inclination and partial detachment of the coating from the substrate near the sample edge. The thickness measurements were determined using Calo tester equipment. The analysis of the nitrogen flow variation did not reveal a significant distinction in the microstructure of the coatings, which aligns with the structure characteristic of Zone T in the SZM model (Ref 21).

Figure 6 displays the diffraction patterns of TiTaZrNb nitride coatings at varying nitrogen flows. The highest intensity peak observed at approximately a diffraction angle 2θ of 41° corresponds to the (200) plane of the FCC cubic phase of (TiTaZrNb)N nitride, exhibiting an average lattice parameter of 4.37 Å (see Table 3). This finding is in good agreement with the research conducted by Shu et al. (Ref 18), who synthesized similar (TiNbZrTa)N coatings through magnetron sputtering at temperatures ranging from 25 and 700 °C, using a constant Ar/N ratio of 97% without applying bias voltage to the substrate. It is noteworthy to observe the change in the crystalline structure of the nitride in comparison with the (TiTaZrNb) matrix, which can be attributed to the occupation of interstitial sites by nitrogen atoms within the matrix. A similar transformation of microstructure from BCC to FCC phase with increasing nitrogen content was reported by Auo during the deposition of (MoNbTaVW)Nx using magnetron sputtering (Ref 31). Furthermore, chang and Chung (Ref 32) deposited multicomponent CrVTiNbZr(N) coatings via evaporation at various nitrogen flows. The metallic CrVTiNbZr coatings exhibited a dominant BCC single-phase structure, whereas the introduction of nitrogen resulted in the formation of dominant FCC structures, such as TiNbN, CrVN and ZrN. These findings are consistent with the appearance of TiN and ZrN reflections at higher nitrogen flows, indicating recrystallization of phases at sufficient nitrogen content. Table 3 shows the values of the crystallite size and lattice parameters of the coatings for the different nitrogen flows used and which were determined by Bragg's law and Scherrer's equation (Ref 33). The slight decrease in the lattice parameter of (TiTaZrNb)N deposited at N_2 flows of 12 sccm and 15 sccm is possibly due to the precipitation of the TiN and ZrN phases that are probably formed by supersaturation of TiTaZrNb with nitrogen.

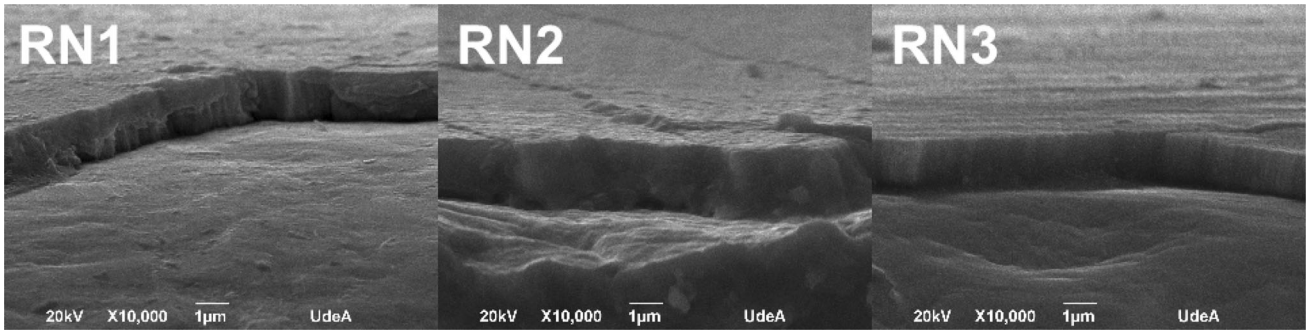


Fig. 5 Cross-sectional SEM images of the deposited (TiTaZrNb)Nx coatings

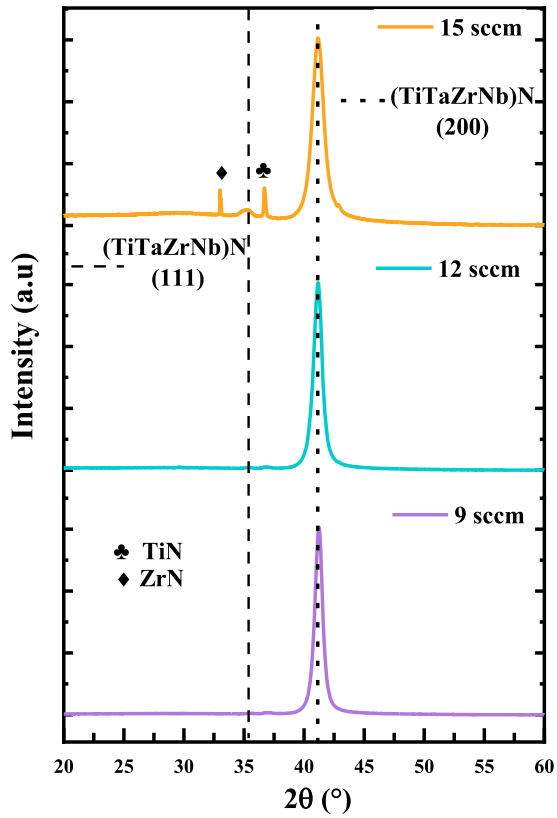


Fig. 6 Diffraction patterns of the (TiTaZrNb)N_x coatings deposited with different nitrogen flows

Table 3 Crystallite size, interplanar distance and lattice parameters of the (TiTaZrNb)Nx coatings

N_2 flow (sccm)	FWHM, °	Crystallite size, nm	Interplanar distance (200), nm	Lattice parameter, nm
9	0.5177	17.13	0.2191	0.4381
12	0.5707	15.54	0.2188	0.4375
15	0.8266	10.73	0.2188	0.4375

Figure 7 shows HRTEM images of the (TiTaZrNb)N deposited at N_2 flow of 12 sccm. FFT of the image confirmed the co-existence of the interplanar distances of the (111) and (200) planes of the face-centered cubic structure of the (TiNbZrTa)N reported by Shu et al (Ref 18). Also, the HRTEM image revealed the presence of grains that growth in different orientations with a typical polycrystalline appearance. Coatings showed preferential growth in (200) plane as confirmed by XRD but as can be seen by TEM, (111) planes can be found.

Figure 8 shows the microhardness results obtained for (TiTaZrNb)Nx coatings deposited under varying nitrogen flows. The hardness of the nitride coatings demonstrates an upward trend with increasing nitrogen flow, reaching its peak value of 23 GPa for the coating deposited at a N_2 flow of 12 sccm. Subsequently, a slight decrease in hardness to 21.7 GPa is observed when the nitrogen flow reaches 15 sccm, which could be attributed to the formation of TiN and ZrN phases.

It is important to note that all three (TiTaZrNb)Nx coatings exhibit significantly higher hardness compared to M2 steel substrates, which has hardness of approximately 6.3 GPa. Furthermore, the (TiTaZrNb)Nx coatings presents higher hardness values when N_2 flows of 12 and 15 sccm are employed compared to the metallic MEA coating. This behavior aligns with the previous observations; for instance, Tsai et al (Ref 34) reported an increase in hardness for (CrHfNbTaTiVZr)N coatings with increasing nitrogen flow. The enhanced hardness is attributed to the formation of nitrides with a high percentage of covalent bonds. Particularly, the variation in hardness observed among the MEA nitride coatings can be attributed to the reduction in crystallite size with increasing N_2 flow, following the Hall–Petch relationship. This phenomenon provides an explanation for the decrease in hardness at a nitrogen flow of 15 sccm, where the crystallite size reaches approximately 10 nm, which is close to the critical size by the Hall–Petch relationship (Ref 35). Also, an increase in residual stresses could be a reason to the increment of hardness as it can be seen in Fig. 9. Tensile-type residual stresses have a value greater than 3 GPa, which normally affect the adherence of the coating to the substrate, since these are added to the shear stresses that originate at the substrate/coating interface, mainly due to the different coefficients of thermal expansion of both materials.

3.3 Tribological Properties of TiTaZrNb and (TiTaZrNb)N_x Coatings

Figure 10 shows the friction coefficient recording of the ball-on-disk test for the (TiTaZrNb)Nx coatings. The coatings deposited with N_2 flows of 9 and 12 sccm exhibited low and comparable friction coefficients of 0.16 and 0.15, respectively. However, the coating deposited with 15 sccm of N_2 showed unstable behavior during the tribological test, displaying an

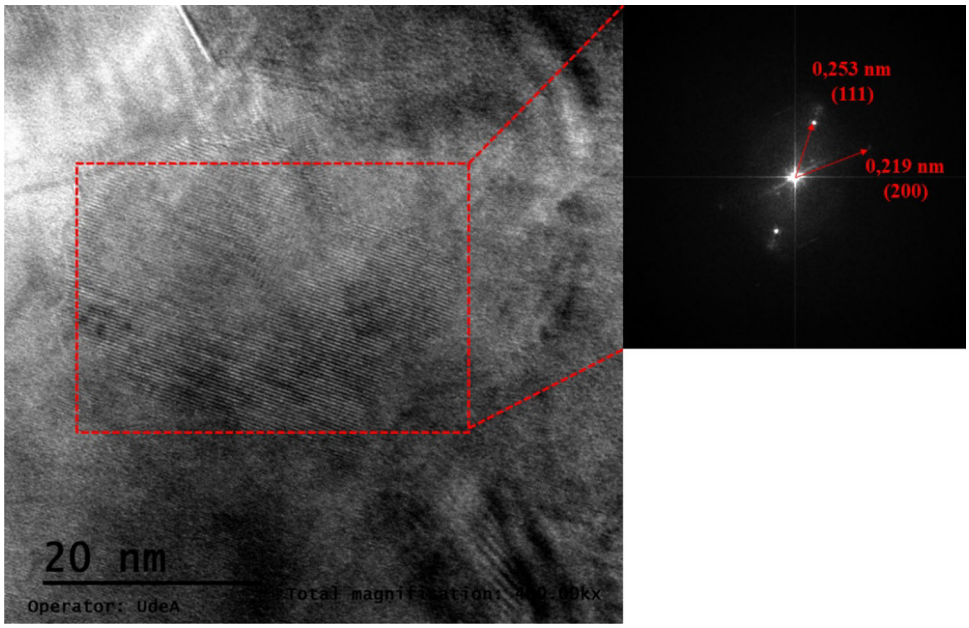


Fig. 7 HRTEM images of the (TiTaZrNb)N deposited at N2 flows of 12 sccm

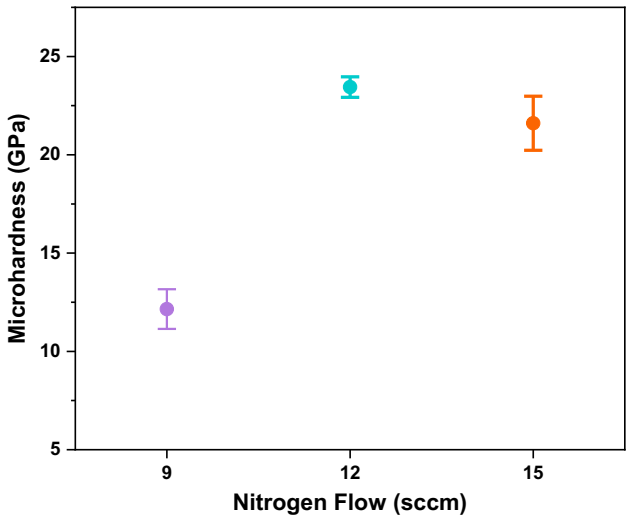


Fig. 8 Microhardness of (TiTaZrNb)Nx coatings

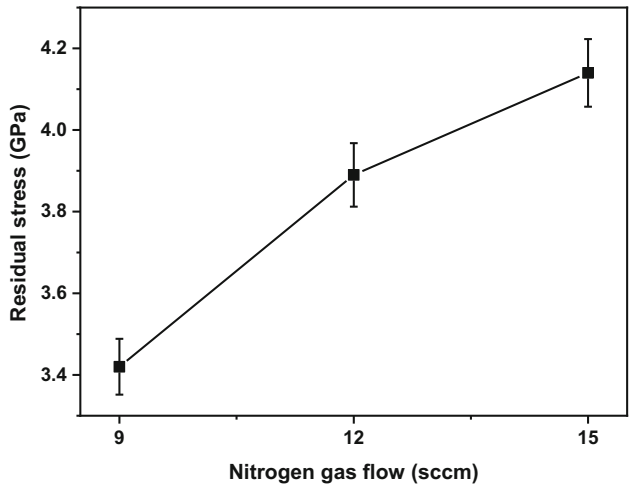


Fig. 9 Tensile-type residual stresses of the (TiTaZrNb)Nx coatings

average coefficient of friction of 0.28 and exhibiting coating detachment, as depicted in Fig. 11. This fact was later confirmed by the evaluation of the wear tracks shown in Fig. 11. Notably, multiple wear stages were observed for the MEA nitride coating deposited at 15 sccm after a sliding distance of approximately 3.5 m. Meanwhile, the MEA nitride coatings deposited with 9 and 12 sccm nitrogen exhibited only one wear mechanism during the steady wear stage (Ref 36). One possible explanation for the observed behavior is the variation in surface roughness and its possible embrittlement due to the greater tensile residual stress of + 4,12 GPa that finally generates the detachment of the coating. The measured roughness values for the MEA nitride coatings were 14, 24.5 and 28.3 nm for the coatings with N_2 flows of 9, 12 and 15 sccm, respectively. It is well-known that rougher surfaces tend to experience more significant wear due to increased friction between surface particles (Ref 29). In this case, higher N_2 flow resulted in coatings with rougher surfaces, which could explain the increased friction coefficient observed in the coating. Thus far, the high level of residual stresses in the coating, as observed in Fig. 9, is the only explanation for its poor adherence and detachment in the tribological test.

The values of the wear rates of the (TiTaZrNb)Nx coatings deposited at three different nitrogen flows are recorded in Table 4 and presented in Fig. 11. The coating deposited with a N_2 flow of 12 sccm exhibited the lowest wear rate of $2x10^{-8}$ mm^3/N.m. The 9 sccm coating had a wear rate of $12x10^{-8}$ mm^3/N.m, while the coating deposited with a flow of 15 sccm showed a wear rate exceeding $15x10^{-8}$ mm^3/N.m and experienced nearly complete detachment from the substrate. However, the wear rates of the first two samples were significantly lower than that of M2 steel, which had a wear rate of $4.6x10^{-6}$ mm^3/N.m, as well as the wear rates reported by other researchers under similar conditions, ranging between $70x10^{-2}$ mm^3/N.m and $3.7x10^{-7}$ mm^3/N.m (Ref 37, 38).

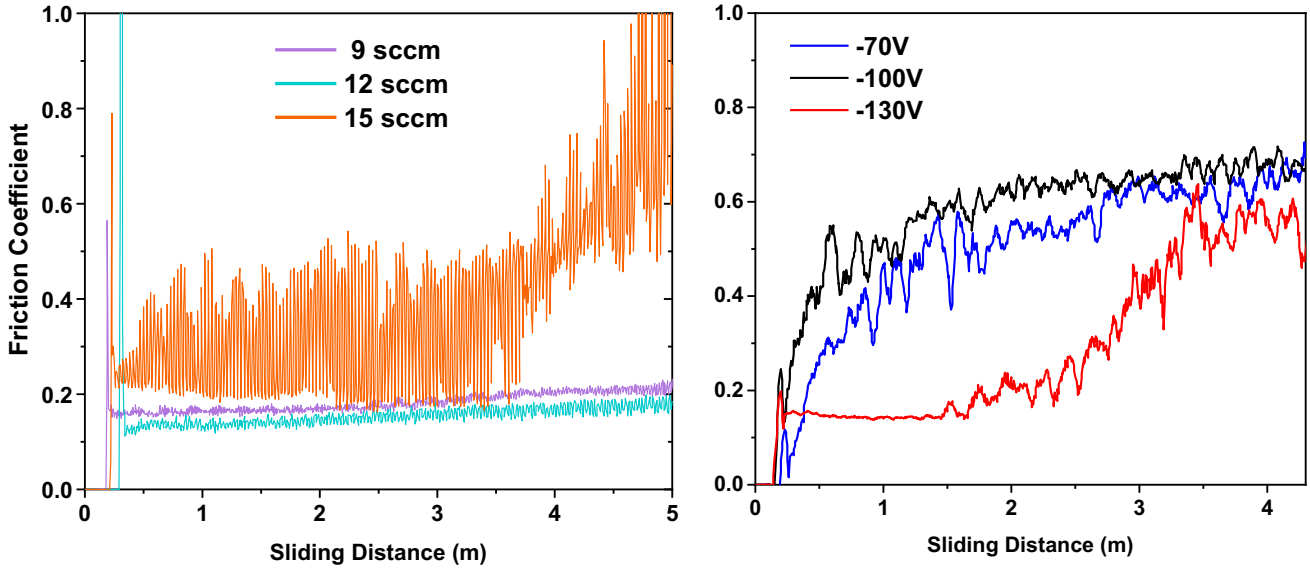


Fig. 10 Friction coefficient of (TiTaZrNb)Nx coatings

These wear rate results correlate well with the hardness measurements, where the coating with higher hardness and lower surface roughness exhibited the lowest wear rate (Ref 29). In a study by Braic et al (Ref 39), TiSiC monolayers and TiSiC/NiC multilayers were deposited on AISI 316 stainless steel and C45 carbon steel substrates by cathodic arc vaporization. The wear rates obtained for these coatings were $2.9x10^{-6}$ mm^3/N and $7x10^{-7}$ mm^3/N, which were also higher than the average wear rates obtained for the (TiTaZrNb)N coatings of this work.

SEM images of the wear tracks of the MEA nitride coatings deposited at 9, 12 and 15 sccm are shown in Fig. 11. Figure 11(a) displays an SEM image of the wear track on the coating deposited with the lowest nitrogen flow of 9 sccm. The image reveals generalized detachments of the coating and an irregular appearance of the wear track, characterized by the presence of cracks and delamination, indicative of abrasive-type wear. A higher magnification inset in the upper right corner provides closer view of these features. Furthermore, a punctual analysis of the elemental composition conducted through EDS within the magnified image, along with the linear EDS analysis, confirms the coexistence of iron and oxygen within the wear track. These elements are found in smaller quantities outside the wear track, suggesting oxidation resulting from the increased temperature generated by friction with the counter body. Additionally, the detachment of the coating in certain areas is attributed to cohesive wear by tribological action. In Fig. 11(b), the wear track of the MEA nitride coating deposited with 12 sccm of nitrogen flow is depicted. The appearance of this wear track is smoother and less pronounced compared to the wear tracks of the coatings deposited at 9 and 15 sccm N_2. No delamination is observed, but small cracks, characteristic of abrasive wear mode and mechanical fatigue wear are present. The presence of iron in the EDS analysis of elemental composition is likely from the steel substrate. Lastly, Fig. 11(c) presents the wear track of the coating deposited with a 15 sccm N_2 flow. This image confirms more severe wear with almost complete detachment of the coating, indicating adhesive-type failure. The elemental composition analysis shows a high percentage of iron, as well as Cr and W, corresponding to the exposed M2 steel substrate. It is worth nothing that all three coatings display signs of tribo-oxidation wear. The tribological behavior of the three coated samples aligns well with the wear rates shown in Table 4.

4. Conclusions

In this study, metallic MEA TiTaZrNb and MEA nitride (TiTaZrNb)Nx coatings were deposited using magnetron sputtering with different bias voltages and nitrogen flows, respectively. Both the TiTaZrNb and (TiTaZrNb)Nx nitride coatings exhibited a columnar growth microstructure. The metallic MEA coating had a cubic BCC structure with preferential growth in the (110) plane, while the nitride MEA coating showed a cubic FCC structure with preferential growth in the (200) plane. This change in crystalline structure from BCC to FCC is attributed to the incorporation of nitrogen into the matrix, resulting in the formation of a solid solution of (TiTaZrNb)N.

Increasing the bias voltage led to apparent densification of the TiTaZrNb metallic MEA coating and an increase in tensile-type residual stresses from 1.8 to 7.2 GPa. The high magnitude of the latter value caused the coating to detach from the substrate a couple of days after being removed from the vacuum chamber.

An increase in hardness and residual stresses was observed with higher nitrogen flow, as nitrogen was incorporated into the (TiTaZrNb) metallic MEA coating. The microhardness of the coated samples ranged between 10.5 and 12.8 GPa for TiTaZrNb and between 12 and 23 GPa for (TiTaZrNb)Nx, significantly higher than the average hardness of 6.3 GPa for M2 steel.

Likewise, the wear rate of the (TiTaZrNb)Nx coating synthesized with a N_2 flow of 12 sccm of $2x10^{-8}$ $mm^3/N.m$ was 4 orders of magnitude lower than metallic coatings MEA and much lower than that of uncoated M2 steel of $4.6x10^{-6}$ mm^3/N, as well as than other hard coatings manufactured by other authors with primarily abrasive wear for all coatings with good wear resistance.

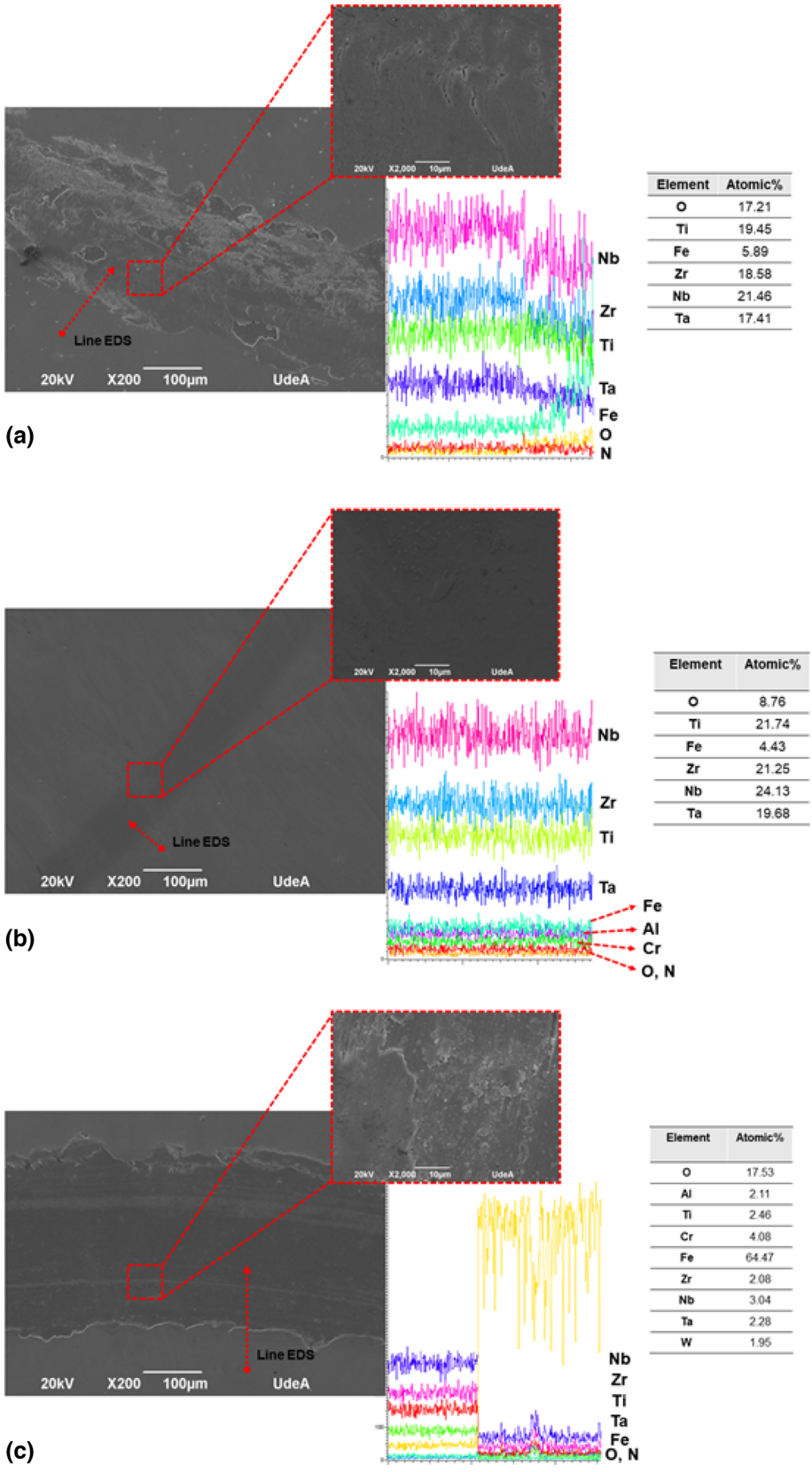


Fig. 11 SEM image of the wear tracks of the MEA nitride coatings deposited with (a) 9, (b) 12, (c) 15 sccm N_2 flow and the corresponding approximate elemental composition by linear EDS

Table 4 Wear rates of coatings obtained

Sample	− 70, V	− 100, V	− 130, V	9, sccm	12, sccm	15, sccm
	Metallic coatings			Nitride coatings		
Wear rate (mm^3/N.m)	$2x10^{-4}$	$8.5x10^{-4}$	$8x10^{-4}$	$12x10^{-8}$	$2x10^{-8}$	Sworn out

Acknowledgment

The authors thank the Vice-Rector for Research of the University of Antioquia for funding this project and the CIDEMAT Research Group for the support for the evaluation and characterization of the synthesized coatings.

Funding

Open Access funding provided by Colombia Consortium.

Conflict of interest

The authors declare that they have no known competing financial interests or personal relationships that could have appeared to influence the work reported in this paper.

Open Access

This article is licensed under a Creative Commons Attribution 4.0 International License, which permits use, sharing, adaptation, distribution and reproduction in any medium or format, as long as you give appropriate credit to the original author(s) and the source, provide a link to the Creative Commons licence, and indicate if changes were made. The images or other third party material in this article are included in the article's Creative Commons licence, unless indicated otherwise in a credit line to the material. If material is not included in the article's Creative Commons licence and your intended use is not permitted by statutory regulation or exceeds the permitted use, you will need to obtain permission directly from the copyright holder. To view a copy of this licence, visit http://creativecommons.org/licenses/by/4.0/.

References

1. J.W. Yeh et al., Nanostructured High-Entropy Alloys with Multiple Principal Elements: Novel Alloy Design Concepts and Outcomes, *Adv. Eng. Mater.*, 2004, **6**(5), p 299–303. https://doi.org/10.1002/adem.200300567
2. W. Hu et al., The Stability and Elasticity in Ta-Ti-V Medium-Entropy Alloys Using First-Principles Calculations, *Front. Mater.*, 2021 https://doi.org/10.3389/fmats.2021.651435
3. X. Yan and Y. Zhang, A Body-Centered Cubic Zr50Ti35Nb15 Medium-Entropy Alloy with Unique Properties, *Scr. Mater.*, 2020, **178**, p 329–333. https://doi.org/10.1016/j.scriptamat.2019.11.059
4. M. Wang et al., Formation and Mechanical Behavior of Body-Centered-Cubic Zr(Hf)-Nb-Ti Medium-Entropy Alloys, *Metall. Mater. Trans. A Phys. Metall. Mater. Sci.*, 2021, **52**(6), p 2100–2110. https://doi.org/10.1007/s11661-021-06263-z
5. C.C. Chang et al., Lattice Distortion or Cocktail Effect Dominates the Performance of Tantalum-Based High-Entropy Nitride Coatings, *Appl. Surf. Sci.*, 2022 https://doi.org/10.1016/j.apsusc.2021.151894
6. B.X. Cao, C. Wang, T. Yang, and C.T. Liu, Cocktail Effects in Understanding the Stability and Properties of Face-Centered-Cubic High-Entropy Alloys at Ambient and Cryogenic Temperatures, *Scr. Mater.*, 2020, **187**, p 250–255. https://doi.org/10.1016/j.scriptamat.2020.06.008
7. J. Li, Y. Huang, X. Meng, and Y. Xie, A Review on High Entropy Alloys Coatings: Fabrication Processes and Property Assessment, *Adv. Eng. Mater.*, 2019, **21**(8), p 1900343. https://doi.org/10.1002/adem.201900343
8. E.P. George, D. Raabe, and R.O. Ritchie, High-Entropy Alloys, *Nat. Rev. Mater.*, 2019, **4**(8), p 515–534. https://doi.org/10.1038/s41578-019-0121-4
9. T. Chen, M. Wong, T. Shun, and J. Yeh, Nanostructured nitride films of multi-element high-entropy alloys by reactive DC sputtering, *Surface Coatings Technology*, 2005, **200**, p 1361–1365. https://doi.org/10.1016/j.surfcoat.2005.08.081
10. V. Novikov, N. Stepanov, S. Zherebtsov, and G. Salishchev, Structure and Properties of High-Entropy Nitride Coatings, *Metals (Basel)*, 2022, **12**(5), p 847. https://doi.org/10.3390/met12050847
11. S.K. Padamata, A. Yasinskiy, V. Yanov, and G. Saevarsdottir, Magnetron Sputtering High-Entropy Alloy Coatings: A Mini-Review, *Metals (Basel)*, 2022, **12**(2), p 319. https://doi.org/10.3390/met12020319
12. Y.-C. Lin, S.-Y. Hsu, Y.-T. Lai, P.-H. Kuo, S.-Y. Tsai, and J.-G. Duh, Effect of the N_2/(Ar+N_2) Ratio on Mechanical Properties of High Entropy Nitride (Cr0.35Al0.25Nb0.12Si0.08V0.20)Nx Films, *Mater. Chem. Phys.*, 2021, **274**, 125195. https://doi.org/10.1016/j.matchemphys.2021.125195
13. X.H. Yan, J.S. Li, W.R. Zhang, and Y. Zhang, A Brief Review of High-Entropy Films, *Mater. Chem. Phys.*, 2018, **210**, p 12–19. https://doi.org/10.1016/j.matchemphys.2017.07.078
14. F. Cemin, S.R.S. de Mello, C.A. Figueroa, and F. Alvarez, Influence of Substrate Bias and Temperature on the Crystallization of Metallic NbTaTiVZr High-Entropy Alloy Thin Films, *Surf. Coatings Technol.*, 2021 https://doi.org/10.1016/j.surfcoat.2021.127357
15. Y. Xu, G. Li, G. Li, F. Gao, and Y. Xia, Effect of Bias Voltage on the Growth of Super-Hard (AlCrTiVZr)N High-Entropy Alloy Nitride Films Synthesized by High Power Impulse Magnetron Sputtering, *Appl. Surf. Sci.*, 2021 https://doi.org/10.1016/j.apsusc.2021.150417
16. M. El Garah, S. Achache, A. Michau, F. Schuster, and F. Sanchette, Structural and Mechanical Properties of AlTiTaZr(-N) Medium Entropy Films (MEF) Obtained by DC Magnetron Sputtering In Dynamic Mode, *Surf. Coatings Technol.*, 2020 https://doi.org/10.1016/j.surfcoat.2020.125941
17. S.K. Bachani, C.J. Wang, B.S. Lou, L.C. Chang, and J.W. Lee, Fabrication of TiZrNbTaFeN High-Entropy Alloys Coatings by HiPIMS: Effect of Nitrogen Flow Rate on the Microstructural Development, Mechanical and Tribological Performance, Electrical Properties and Corrosion Characteristics, *J. Alloys Compd.*, 2021 https://doi.org/10.1016/j.jallcom.2021.159605
18. R. Shu et al., Microstructure and Mechanical, Electrical, and Electrochemical Properties of Sputter-Deposited Multicomponent (TiNbZrTa)Nx Coatings, *Surf. Coatings Technol.*, 2020, **389**, 125651. https://doi.org/10.1016/j.surfcoat.2020.125651
19. G.G. Stoney, The tension of metallic films deposited by electrolysis, in *Proceedings of the Royal Society of London. Series A, Containing Papers of a Mathematical and Physical Character*, **82** (553), 172–175 (1909). https://doi.org/10.1098/rspa.1909.0021
20. ASTM International - Standards Worldwide, ASTM G99-17 Standard test method for wear testing with a pin-on-disk apparatus, (2017). https://www.astm.org/g0099-17.html
21. J.A. Thornton, The Microstructure of Sputter-Deposited Coatings, *J. Vac. Sci. Technol. A Vacuum. Surfaces Film.*, 1986, **4**(6), p 3059–3065. https://doi.org/10.1116/1.573628

22. E. Kusano, Structure-Zone Modeling of Sputter-Deposited Thin Films: A Brief Review, *Appl. Sci. Converg. Technol.*, 2019, **28**(6), p 179–185. https://doi.org/10.5757/asct.2019.28.6.179
23. W. Dai and Y. Shi, Effect of Bias Voltage on Microstructure and Properties of Tantalum Nitride Coatings Deposited by RF Magnetron Sputtering, *Coatings*, 2021, **11**(8), p 911. https://doi.org/10.3390/coatings11080911
24. J.-F. Tang, C.-Y. Lin, F.-C. Yang, and C.-L. Chang, Influence of Nitrogen Content and Bias Voltage on Residual Stress and the Tribological and Mechanical Properties of CrAlN Films, *Coatings*, 2020, **10**(6), p 546. https://doi.org/10.3390/coatings10060546
25. H. Guan et al., Laser-Clad Nb(Ta)TiZr Medium-Entropy Alloy Coatings on Pure Zr Sheet: Microstructural Characteristics, Hardness and Wear Resistance, *Intermetallics*, 2022 https://doi.org/10.1016/j.intermet.2022.107498
26. S. Achache, A. Alhussein, B. Guelorget, R. Salut, M. François, and F. Sanchette, Effect of Oxygen Addition on Microstructure and Mechanical Properties of Quaternary TNTZ Superelastic Thin Films Obtained by Magnetron Sputtering, *Mater. Chem. Phys.*, 2018, **217**, p 262–269. https://doi.org/10.1016/j.matchemphys.2018.06.066
27. L.S. Qiu, X.D. Zhu, and K.W. Xu, Internal Stress on Adhesion of Hard Coatings Synthesized by Multi-Arc Ion Plating, *Surf. Coatings Technol.*, 2017, **332**, p 267–274. https://doi.org/10.1016/j.surfcoat.2017.07.076
28. X. Feng, G. Tang, L. Gu, X. Ma, M. Sun, and L. Wang, Preparation and Characterization of TaNbTiW Multi-Element Alloy Films, *Appl. Surf. Sci.*, 2012, **261**, p 447–453. https://doi.org/10.1016/j.apsusc.2012.08.030
29. X. Zhang et al., Effect of Bias Voltages on Microstructure and Properties of (TiVCrNbSiTaBY)N High Entropy Alloy Nitride Coatings Deposited by RF Magnetron Sputtering, *Vacuum*, 2022, **195**, 110710. https://doi.org/10.1016/j.vacuum.2021.110710
30. N.J. Petch, The Cleavage Strength of Polycrystals, *J. Iron Steel Inst.*, 1952, **174**, p 25–28
31. A. Xia, R. Dedoncker, O. Glushko, M.J. Cordill, D. Depla, and R. Franz, Influence of the Nitrogen Content on the Structure and Properties of MoNbTaVW High Entropy Alloy Thin Films, *J. Alloys Compd.*, 2021, **850**, 156740. https://doi.org/10.1016/j.jallcom.2020.156740
32. Y.Y. Chang and C.H. Chung, Tribological and Mechanical Properties of Multicomponent CrVTiNbZr(N) Coatings, *Coatings*, 2021, **11**(1), p 1–16. https://doi.org/10.3390/coatings11010041
33. L.J. Cardenas-Flechas, C.P. Mejía-Villagran, M. Rincon-Joya, and J.J. Olaya-Florez, Synthesis of Nanostructured (Ti-Zr-Si)N Coatings Deposited on Ti6Al4V Alloy, *Rev. la Acad. Colomb. Ciencias. Exactas Físicas Nat.*, 2021, **45**(175), p 570–581. https://doi.org/10.18257/raccefyn.1198
34. D. Tsai, E. Chen, Z. Chang, and F. Shieu, Mechanical, and Electrical Properties of (CrHfNbTaTiVZr) N Coatings Deposited by Reactive Magnetron Sputtering, *Coatings*, 2022 https://doi.org/10.3390/coatings12040437
35. C.H. Lai, S.J. Lin, J.W. Yeh, and A. Davison, Effect of Substrate Bias on the Structure and Properties of Multi-Element (AlCrTaTiZr)N Coatings, *J. Phys. D Appl. Phys.*, 2006, **39**(21), p 4628–4633. https://doi.org/10.1088/0022-3727/39/21/019
36. J. Li, Y. Chen, Y. Zhao, X. Shi, S. Wang, and S. Zhang, Super-Hard (MoSiTiVZr)Nx High-Entropy Nitride Coatings, *J. Alloys Compd.*, 2022, **926**, p 166807. https://doi.org/10.1016/j.jallcom.2022.166807
37. L.H. Portela de Abreu et al., The Effect of Cathodic Cage Plasma TiN Deposition on Surface Properties of Conventional Plasma Nitrided AISI-M2 Steel, *Metals (Basel)*, 2022, **12**(6), p 961. https://doi.org/10.3390/met12060961
38. L.A. Ardila Rodríguez, J.J. Olaya Flórez, and J.M. Arroyo Osorio, Microstructure, Morphology, Adhesion and Tribological Behavior of Sputtered Niobium Carbide and Bismuth Films on Tool Steel, *Ing. e Investig.*, 2014, **34**(3), p 12–18. https://doi.org/10.15446/ing.investig.v34n3.41938
39. M. Braic, M. Balaceanu, A.C. Parau, M. Dinu, and A. Vladescu, Investigation of Multilayered TiSiC/NiC Protective Coatings, *Vacuum*, 2015, **120**, p 60–66. https://doi.org/10.1016/j.vacuum.2015.06.019

Publisher's Note Springer Nature remains neutral with regard to jurisdictional claims in published maps and institutional affiliations.